



Cite this: *Chem. Sci.*, 2017, 8, 4242

Hybrid photocathode consisting of a CuGaO₂ p-type semiconductor and a Ru(II)–Re(I) supramolecular photocatalyst: non-biased visible-light-driven CO₂ reduction with water oxidation†

Hiromu Kumagai,^a Go Sahara,^a Kazuhiko Maeda,^a Masanobu Higashi,^b Ryu Abe^b and Osamu Ishitani^{*,a}

A CuGaO₂ p-type semiconductor electrode was successfully employed for constructing a new hybrid photocathode with a Ru(II)–Re(I) supramolecular photocatalyst (RuRe/CuGaO₂). The RuRe/CuGaO₂ photocathode displayed photoelectrochemical activity for the conversion of CO₂ to CO in an aqueous electrolyte solution with a positive onset potential of +0.3 V vs. Ag/AgCl, which is 0.4 V more positive in comparison to a previously reported hybrid photocathode that used a NiO electrode instead of CuGaO₂. A photoelectrochemical cell comprising this RuRe/CuGaO₂ photocathode and a CoO_x/TaON photoanode enabled the visible-light-driven catalytic reduction of CO₂ using water as a reductant to give CO and O₂ without applying any external bias. This is the first self-driven photoelectrochemical cell constructed with the molecular photocatalyst to achieve the reduction of CO₂ by only using visible light as the energy source and water as a reductant.

Received 1st March 2017

Accepted 5th April 2017

DOI: 10.1039/c7sc00940b

rsc.li/chemical-science

Introduction

The use of artificial photosynthesis, particularly for the photochemical reduction of CO₂, has gained much attention because it might provide solutions for overcoming both the problem of global warming and the shortage of fossil resources. Metal complex photocatalysts have been intensively developed for achieving the reduction of CO₂ using the energy of visible light with a high selectivity for the products.^{1–3} In particular, supramolecular photocatalysts composed of both redox photosensitizer and catalyst units have exhibited high selectivity, durability, and efficiency for the reduction of CO₂ under visible light conditions even in aqueous solutions,^{4,5} as well as in organic solvents.^{6–14} In these photocatalytic reactions, sacrificial reductants such as 1-benzyl-1,4-dihydronicotinamide,⁷ sodium ascorbate,⁴ and 2-(1,3-dimethyl-2,3-dihydro-1*H*-benzimidazol-2-yl)benzoic acid⁵ are necessary because of the low oxidizing power of the photosensitizer unit, which cannot sufficiently oxidize water, an abundant electron donor.

Hybrid photocatalysts and photoelectrodes composed of metal complexes and semiconductor materials with relatively

high photochemical oxidizing power, in which the metal complexes act as catalysts alone in some cases^{15–24} but as photocatalysts in others,^{25–30} have recently been studied for the visible-light-driven photocatalytic reduction of CO₂. In the cases where metal complexes are used as photocatalysts, hybrid photocatalysts with semiconductor particles can cope with both the high selectivity of the CO₂ reduction and the strong oxidation power *via* the step-by-step excitation of both the redox photosensitizer unit of the metal complex photocatalyst and the semiconductor, so-called Z-scheme mechanism. However, visible-light-driven CO₂ reduction accompanied by water oxidation has not been achieved yet using hybrids with these particle systems. We have previously reported a hybrid photocathode consisting of a Ru(II)–Re(I) supramolecular photocatalyst (RuRe) fixed on a NiO p-type semiconductor electrode for the photoelectrochemical reduction of CO₂.³¹ In this system, the metal complex photocatalyst can drive the reduction of CO₂ by the injection of electrons from an external electric circuit through the NiO semiconductor electrode without the addition of any sacrificial electron sources. This RuRe/NiO photoelectrochemical system was used to successfully achieve the catalytic reduction of CO₂ using water as an electron source, combined with a CoO_x/TaON n-type semiconductor photoanode for the oxidation of water.³² However, the performance of this photoelectrochemical cell was still insufficient, *i.e.*, the combined photoelectrochemical cell needed the assistance of an external electrical bias (0.3 V) and a chemical bias (0.10 V) produced by a difference in pH, and the photoelectrochemical cell generated much lower yields of the

^aDepartment of Chemistry, School of Science, Tokyo Institute of Technology, O-okayama 2-12-1-NE-1, Meguro-ku, Tokyo 152-8550, Japan. E-mail: ishitani@chem.titech.ac.jp

^bDepartment of Energy and Hydrocarbon Chemistry, Graduate School of Engineering, Kyoto University, Katsura, Nishikyo-ku, Kyoto 615-8510, Japan

† Electronic supplementary information (ESI) available. See DOI: 10.1039/c7sc00940b



reduction products (CO and H₂) compared to the oxidation one (O₂) from the viewpoint of electron balance.

One of the main reasons for these insufficiencies was the low activity of the NiO electrode. Although NiO has been widely used as an electrode material for p-type dye-sensitized photocathodes, the flat band position of NiO is relatively negative (+0.34 V vs. Ag/AgCl in a saturated aqueous solution of KCl at a pH of 7).³³ This could cause a large loss of energy for passing an electron to the excited state of the Ru(II) photosensitizer unit ($E_{1/2} = +0.51$ V vs. Ag/AgCl)³¹ through the interface, leading to the requirement of a large external bias (totally 0.4 V) when this photocathode is used for constructing a photoelectrochemical cell combined with a photoanode. The consumption of electrons for reducing trivalent nickel ions (Ni³⁺) that originally existed in NiO could also be problematic because it lowers the Faraday efficiencies of the reduction reactions on the photocathode.^{31,32,34} Therefore, the development of new p-type semiconductor electrodes is necessary for the field of hybrid photoelectrochemical cells with supramolecular photocatalysts for reduction of CO₂.

Here, we report a novel hybrid photocathode (**RuRe**/CuGaO₂) consisting of CuGaO₂ as the p-type semiconductor electrode and **RuRe** as the photocatalyst for the reduction of CO₂. CuGaO₂ with a delafossite crystal structure is known to exhibit p-type semiconducting properties that are derived from native Cu⁺ vacancies.³⁵ It has received attention as a transparent conducting oxide material^{36–38} and has also been studied as an alternative to NiO for dye-sensitized photocathodes due to both its high conductivity (10⁻¹–10⁻² S cm⁻¹)³⁸ and positive flat band potential, which was reported to be approximately 0.16 V more positive compared to that of NiO.^{39,40} Although CuGaO₂ electrodes have been investigated as parts of dye-sensitized solar cells, to the best of our knowledge there are no reports on the application of CuGaO₂ electrodes for photocatalytic reactions such as CO₂ reduction and H₂ evolution. The onset potential for the reduction of CO₂ by the as-synthesized **RuRe**/CuGaO₂ was revealed to be 0.4 V more positive in comparison to that of the **RuRe**/NiO electrode. A photoelectrochemical cell consisting of **RuRe**/CuGaO₂ and a CoO_x/TaON photoanode enabled the visible-light-driven catalytic reduction of CO₂ using water as the reductant without applying any external bias.

Results and discussion

Preparation of the **RuRe**/CuGaO₂ photocathode

CuGaO₂ powder was prepared using a solid-state reaction method. The XRD pattern of the synthesized powder revealed that the delafossite structure of the CuGaO₂ was obtained with no obvious impurity phase (Fig. S1†). The UV-vis diffuse reflectance spectrum of the synthesized CuGaO₂ powder indicated that the powder absorbs light at $\lambda < 460$ nm, which has been reported in previous research into CuGaO₂ powder (Fig. S2†).^{41,42} The CuGaO₂ electrodes were prepared by drop-casting a powder suspension onto FTO glass substrates following an annealing with a N₂ flow. SEM observations revealed that the polycrystalline CuGaO₂ particles had rod-like shapes on the micron scale and the thickness of the stacked CuGaO₂ particle layer of the electrode was approximately 15 μ m

(Fig. S3†). The dominant material at the solid-liquid interface of the electrode should be the deposited CuGaO₂ particles and not the underlying flat FTO film. **RuRe** and its model complexes (**Ru** and **Re**) (see Chart 1) were synthesized in accordance with reported procedures.⁴³ A CuGaO₂ electrode was immersed in an acetonitrile solution containing the metal complex overnight to obtain hybridized photocathodes.

Photoelectrochemical properties of the **RuRe**/CuGaO₂ photocathode

The photoelectrochemical properties of the synthesized **RuRe**/CuGaO₂ electrode were investigated under irradiation at $\lambda_{\text{ex}} > 460$ nm, which can be selectively absorbed by the Ru photosensitizer unit of **RuRe**, in an aqueous solution containing NaHCO₃ (50 mM) saturated with CO₂, which was used as the supporting electrolyte. Fig. 1(a) shows the current-potential curves of the **RuRe**/CuGaO₂ electrode under continuous visible-light irradiation ($\lambda_{\text{ex}} > 460$ nm) and under dark conditions. This clearly indicates that the **RuRe**/CuGaO₂ electrode generated a cathodic photocurrent under irradiation. The difference in the observed current between the irradiation and dark conditions indicated that the cathodic photoresponse of the **RuRe**/CuGaO₂ electrode started at approximately +0.3 V vs. Ag/AgCl (equivalent to +0.9 V vs. RHE). It should be noted that this onset potential of the photocurrent was approximately 0.4 V more positive than that of **RuRe**/NiO (*ca.* -0.1 V, Fig. 1(b)).³¹ A pristine CuGaO₂ electrode showed a slight cathodic photoresponse (*ca.* -1 μ A cm⁻²) under irradiation at $\lambda_{\text{ex}} > 460$ nm (Fig. S4†), which was almost negligible compared to the photocurrent from the **RuRe**/CuGaO₂ electrode, as shown in Fig. 1(a). The anodic current obtained from *ca.* +0.2 V vs. Ag/AgCl in the dark was derived from the self-oxidation of the CuGaO₂ surface⁴² but not from the redox reaction of the immobilized **RuRe**.

Fig. 2 shows the dependence of the IPCE of the **RuRe**/CuGaO₂ electrode and a bare CuGaO₂ electrode without **RuRe** on the wavelength of light used for irradiation when the applied potential was -0.3 V vs. Ag/AgCl. The diffuse reflectance spectra of these electrodes are also shown in Fig. 2. The **RuRe**/CuGaO₂ electrode displayed light absorption up to 600 nm, which was derived from the **Ru** photosensitizer unit of the hybridized

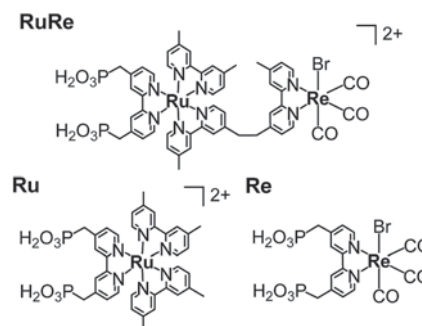


Chart 1 Structures and abbreviations of the Ru(II)–Re(I) supramolecular photocatalyst (**RuRe**) and its model mononuclear metal complexes used as the photosensitizer unit (**Ru**) and the catalyst unit (**Re**).



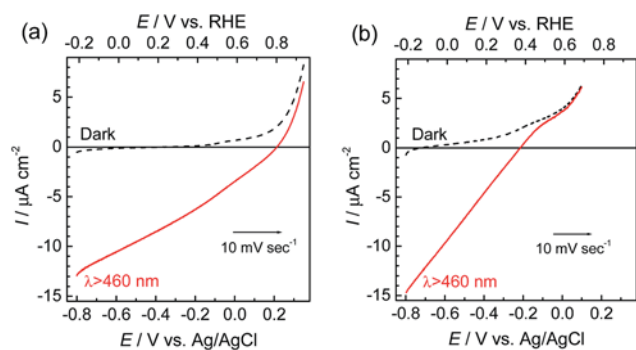


Fig. 1 Current–potential curves of RuRe/CuGaO₂ (a) and RuRe/NiO₃₁ (b) electrodes under continuous visible-light irradiation ($\lambda_{\text{ex}} > 460$ nm) and under dark conditions. A 50 mM aqueous solution of NaHCO₃ (pH 6.6) saturated with CO₂ was used as the electrolyte.

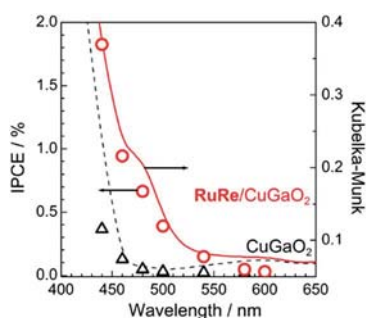


Fig. 2 Dependence on wavelength of the incident-photon-to-current efficiencies of the RuRe/CuGaO₂ (red circles) and bare CuGaO₂ (black triangles) electrodes at -0.3 V vs. Ag/AgCl. An aqueous solution containing 50 mM NaHCO₃ saturated with CO₂ was used as the electrolyte (pH 6.6). The diffuse reflectance spectra of these electrodes are also shown: RuRe/CuGaO₂ (red solid line) and CuGaO₂ (black broken line).

RuRe. In the case of the RuRe/CuGaO₂ electrode, the dependence agreed well with the absorption spectrum of the electrode, whereas the bare CuGaO₂ electrode exhibited almost no photoresponse under irradiation at $\lambda_{\text{ex}} > 460$ nm. The flat band potential of the CuGaO₂ electrode in the reaction solution was estimated using electrochemical impedance spectroscopy (Fig. S5[†]) to be +0.47 V, which was more negative than the reduction potential of the excited state of RuRe ($E_{1/2}^{\text{red}} = +0.49$ V).⁴⁴ These results obviously indicate that the photocurrent was induced by the injection of the electrons from the CuGaO₂ electrode into the excited Ru photosensitizer unit of RuRe, as shown in Fig. 3. To conclude this section, we successfully synthesized the new hybrid photocathode (RuRe/CuGaO₂) for the reduction of CO₂ with an onset potential that was approximately 0.4 V more positive in comparison to that reported for the RuRe/NiO photocathode.

Photoelectrochemical reduction of CO₂ using the RuRe/CuGaO₂ photocathode

The gas products were analyzed during the continuous visible-light irradiation ($\lambda_{\text{ex}} > 460$ nm) of the RuRe/CuGaO₂

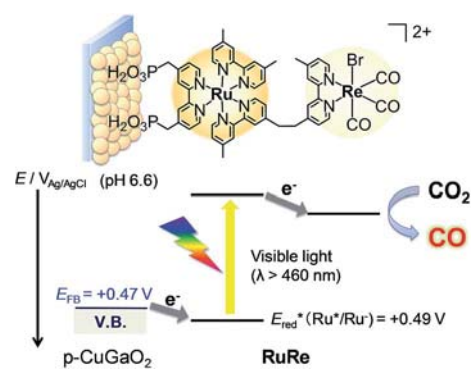


Fig. 3 Reaction scheme of the reduction of CO₂ by the RuRe/CuGaO₂ hybrid photocathode.

photocathode in an aqueous solution saturated with CO₂ in the presence of an applied potential. Fig. 4 shows the time courses of both the produced CO and H₂, and a half amount of electrons passing at an applied potential of -0.3 V vs. Ag/AgCl. After irradiating for 15 h, 966 nmol of CO and 622 nmol of H₂ were detected as the reduction products when the turnover number for the formation of CO (TON_{CO}), which was based on the RuRe deposited on the electrode, was 125, and the total faradaic efficiency for the production of the reduced products (CO + H₂) was 81%. In the irradiated solution, HCOOH was not detected (the detection limit of the capillary electrophoresis system used was 2 μmol). An isotope tracer experiment using ¹³CO₂ and NaH¹³CO₃ was also conducted to confirm the source of the carbon for the produced CO. GC-MS analysis using NaH¹³CO₃ as the electrolyte under a ¹³CO₂ atmosphere revealed that ¹³CO was the main product of the reaction with a very small proportion of ¹²CO, where the ¹³C content was 99% in both ¹³CO₂ and NaH¹³CO₃ (Fig. 5(a)). It is worth noting that the Re unit of RuRe has three ¹²CO ligands, and the exchange of the ¹²CO ligands with ¹³CO proceeded in the photocatalytic ¹³CO₂ reduction reactions in homogeneous systems. On the other hand, only ¹²CO was detected in the gas phase of the reaction using ordinary CO₂ and NaHCO₃ (Fig. 5(b)). These results clearly indicate that the source of carbon for CO was CO₂.

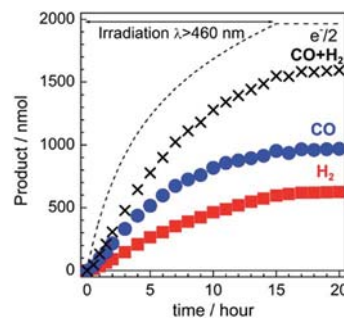


Fig. 4 Time courses of the chemical products (CO and H₂) and a half amount of electrons passing through the RuRe/CuGaO₂ photocathode under continuous visible-light irradiation ($\lambda_{\text{ex}} > 460$ nm) at -0.3 V vs. Ag/AgCl. A 50 mM aqueous solution of NaHCO₃ (pH 6.6) that was saturated with CO₂ was used as the electrolyte.



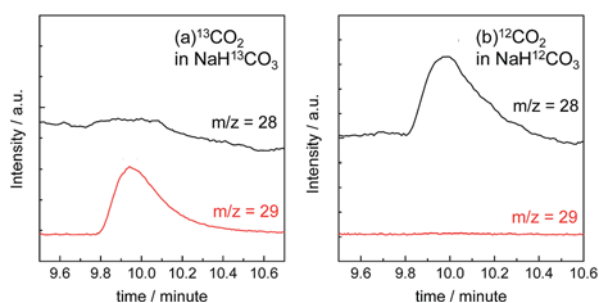


Fig. 5 GC-MS chromatograms of the gas products in the reaction chamber after irradiation (the detected $m/z = 28$ for ^{12}C and 29 for ^{13}C). The **RuRe**/CuGaO₂ photocathode was irradiated at $\lambda_{\text{ex}} > 460$ nm in an aqueous solution containing 50 mM sodium bicarbonate (pH 6.6) at -0.7 V vs. Ag/AgCl for 5 h using $^{13}\text{CO}_2$ and $\text{NaH}^{13}\text{CO}_3$ (a) and ordinary CO_2 and NaHCO_3 (b).

Table 1 shows the results of the photoelectrochemical reactions that were conducted under various conditions. The **RuRe**/CuGaO₂ electrode could produce CO as the main product with H₂ under visible-light irradiation at an applied potential from -0.1 V to -0.7 V vs. Ag/AgCl (Table 1, entries 1–3). The TON_{CO} of the **RuRe**/CuGaO₂ electrode was more than twice the reported value of the **RuRe**/NiO electrode (32; entry 10), even at more positive potentials, *i.e.*, -0.3 V and -0.1 V. Carbon monoxide was not produced under an Ar atmosphere even when the same photocathode was used, whereas H₂ was produced (entry 4). The reactions using the bare CuGaO₂ electrode or electrodes with only one of the model mononuclear complexes, *i.e.*, **Ru** or **Re**, did not lead to the formation of any CO (entries 5, 6, 7 and 8). In these cases, almost negligible or small amounts of H₂ were produced during the irradiation. Therefore, the CuGaO₂ electrode, the **RuRe** supramolecular photocatalyst, and a CO₂ atmosphere may all be required for the photoelectrochemical reduction of CO₂. We note that an electrode that was loaded with both the model complexes (**Re** and **Ru**) at random produced a much smaller amount of CO (entry 9), which indicates that the molecular design of **RuRe**, which enables the

sufficiently efficient transfer of electrons from the reduced photosensitizer unit to the catalyst unit, is quite important for developing photocathodes for the reduction of CO₂.

As was described above, the production of H₂ was detected using the **RuRe**/CuGaO₂ photocathode in reactions under both Ar and CO₂ atmospheres, whereas only a small amount of H₂ was produced in the case of **RuRe**/NiO. It has been reported that the decomposition products of both the **Ru** photosensitizer unit in systems using **RuRe** supramolecular photocatalysts and **Ru** in a mixed system of **Ru** and **Re**, *i.e.*, a complex of the form $[\text{Ru}^{\text{II}}(\text{N}^{\wedge}\text{N})_2(\text{solvent})_2]^{n+}$ ($\text{N}^{\wedge}\text{N}$ = diimine ligand), were gradually produced during the photocatalytic reactions, and these acted as catalysts for both the evolution of H₂ and the formation of HCOOH from CO₂.^{5,45} However, the **Ru**/CuGaO₂ photocathode produced a smaller amount of H₂ than that of the **RuRe**/CuGaO₂ photocathode. Therefore, the generation of H₂ might result not only from the decomposition products of **RuRe** but also from the coexistence of photoexcited **RuRe** on the CuGaO₂ surface. Because it has been reported that CuGaO₂ worked as a H₂-evolving photocathode under UV light irradiation (CuGaO₂ itself can absorb UV light),⁴² back electron transfer from photoexcited **RuRe** to the CuGaO₂ surface, which could act as an active site of H₂ evolution, might induce the production of H₂. Detailed studies of the reaction mechanism of the production of H₂ and its suppression are in progress in our laboratory.

Fig. 6 shows the time courses of the photocurrent using the **RuRe**/CuGaO₂ photocathode at the potentials of -0.1 V, -0.3 V, and -0.7 V vs. Ag/AgCl under irradiation at $\lambda_{\text{ex}} > 460$ nm, which correspond to entries 1–3 in Table 1. In all of the cases, a photocurrent was observed even after irradiation for 15 h. However, the photocurrent decreased in the first stage of the photoelectrochemical reaction, and the rates of formation of CO and H₂ also became slower in accordance with the decline in the photocurrent (Fig. 4 for the case at -0.3 V; Fig. S6† for the other cases). To confirm the reasons for the decline in the photocurrent and the rates of product formation, an estimation of the amount of “electrochemically active” **RuRe** species on the CuGaO₂ surface was conducted using cyclic voltammetry in an

Table 1 Photoelectrochemical reactions using various electrodes under various conditions^a

Entry	Sample	Complex/nmol	Potential ^b /V	Products		
				CO/nmol (TON_{CO})	H ₂ /nmol	$F_{\text{red}}^f/\%$
1	RuRe /CuGaO ₂	7.9	-0.7	668(85)	387	68
2	RuRe /CuGaO ₂	7.7	-0.3	966(125)	622	81
3	RuRe /CuGaO ₂	9.3	-0.1	781(84)	494	72
4 ^c	RuRe /CuGaO ₂	8.3	-0.3	n.d. ^g	346	52
5	CuGaO ₂	—	-0.7	n.d. ^g	25	7
6	CuGaO ₂	—	-0.3	n.d. ^g	Trace	—
7	Ru /CuGaO ₂	9.6	-0.3	n.d. ^g	64	20
8	Re /CuGaO ₂	14.2	-0.3	n.d. ^g	25	13
9 ^d	(Ru , Re)/CuGaO ₂	Re: 11.1, Ru: 4.4	-0.3	35(3, based on Re)	31	34
10 ^e	RuRe /NiO ³²	11.2	-0.7	361(32)	36	64

^a The electrode was irradiated at $\lambda_{\text{ex}} > 460$ nm using a 300 W Xe lamp for 15 h. A 50 mM aqueous solution of NaHCO₃ was used as the electrolyte.

^b Versus Ag/AgCl (sat. KCl). ^c Under an Ar atmosphere. ^d The electrode was prepared *via* immersion in solutions of **Re** and **Ru** in sequence. ^e Data from ref. 32 (irradiated for 12 h). ^f F_{red} : Faradaic efficiency for reduction reaction. ^g n.d.: not detected.



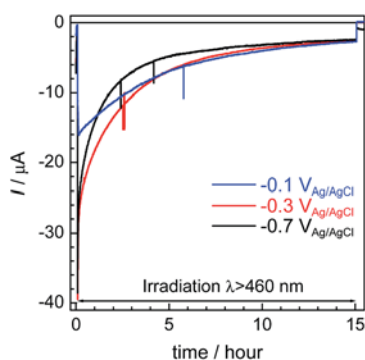


Fig. 6 Time courses of the photocurrent using the **RuRe**/**CuGaO₂** photocathode at various potentials (corresponding to entries 1–3 in Table 1) under irradiation at $\lambda_{\text{ex}} > 460$ nm.

acetonitrile solution (Fig. S7 and Table S1†) according to reported procedures, where the areas of the oxidation peaks of **Ru^{II}/Ru^{III}** were used for the estimation.³² This indicated that about 80% of the **RuRe** lost its electrochemical activity after reacting for 15 h, which was probably due to (photo)desorption and/or photodecomposition of **RuRe** and could account for the decline in the photocurrent and the photocatalytic activity. In addition, the difference between the peak potentials of the redox reaction of **Ru^{II}/Ru^{III}** was greater after the reaction (Fig. S7†), which indicates that the ohmic resistance of the electrode increased. Because the XPS measurements of the electrodes showed no obvious change in the electronic states of the Cu and Ga on the surface of the **CuGaO₂** particles during the reaction (Fig. S8†), the increase in the internal resistance of the **CuGaO₂** electrode might not be caused by the collapse of the **CuGaO₂** surface. An increase in inter-particle resistance probably proceeded in the electrode owing to the gradual deterioration of physical contact among the **CuGaO₂** particles. This might induce the deactivation of the photocathode. We note that the peaks of Ru and Re in the XPS measurements were too small to be identified, possibly due to the low loading density of **RuRe** on **CuGaO₂**.

Photoelectrochemical reduction of CO₂ using a hybrid electrochemical cell with a Z-scheme configuration

To couple the photoelectrochemical reduction of CO₂ to the oxidation of water, the **CoO_x/TaON** photoanode, which has been reported to be an efficient photoanode for the water oxidation reaction, was examined as the counter photoanode in a full photoelectrochemical cell using the **RuRe**/**CuGaO₂** hybrid photocathode. The **CoO_x/TaON** electrode was prepared according to a previously reported method.⁴⁶ Fig. 7 shows the current–potential curve of the **CoO_x/TaON** photoanode in a 50 mM aqueous solution of NaHCO₃ with a pH of 6.6 that was purged with CO₂, which is the same electrolyte as was used for the photocathode. An anodic photocurrent was clearly observed, as in the cases of the aqueous solutions of Na₂SO₄ (pH 8) and NaHCO₃ (pH 8.3), that were both purged with Ar.⁴⁶ In addition, the evolution of O₂ under visible-light irradiation in a 50 mM aqueous solution of NaHCO₃ purged with CO₂ was confirmed by

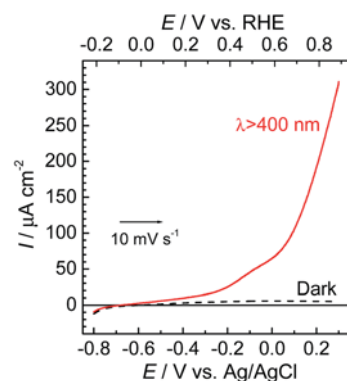


Fig. 7 Current–potential curves of the **CoO_x/TaON** photoanode under continuous visible-light irradiation ($\lambda_{\text{ex}} > 400$ nm) and under dark conditions. A 50 mM aqueous solution of NaHCO₃ (pH 6.6) saturated with CO₂ was used as the electrolyte.

the analysis of the gas products at an applied potential of +0.2 V vs. Ag/AgCl, and its total faradaic efficiency was 93% after irradiating for 60 min (Fig. S9†).

Fig. 8 shows a schematic representation of the hybrid photoelectrochemical cell consisting of the **RuRe**/**CuGaO₂** photocathode and the **CoO_x/TaON** photoanode in a Z-scheme configuration. Two chambers containing the electrolyte solution purged with CO₂ were separated by a Nafion membrane, and one photoelectrode was installed in each chamber. Visible light with $\lambda_{\text{ex}} > 460$ nm and $\lambda_{\text{ex}} > 400$ nm was used to irradiate the **RuRe**/**CuGaO₂** photocathode and the **CoO_x/TaON** photoanode, respectively. It is worth nothing that the photoelectrochemical reaction was conducted under short-circuit conditions with the same electrolyte for both electrodes, *i.e.*, there was no external electrical or chemical bias between the electrodes. In addition, a higher intensity of irradiated light was utilized for the photocathode (4.5×10^{17} photon $\text{cm}^{-2} \text{s}^{-1}$ in the wavelength range 460–600 nm) than that for the photoanode (4.1×10^{16} photon $\text{cm}^{-2} \text{s}^{-1}$ in the wavelength range 400–600 nm) to achieve sufficient photoexcitation of the loaded **RuRe** on the photocathode.

Photoelectrolysis using the constructed photoelectrochemical cell was conducted with intermittent visible-

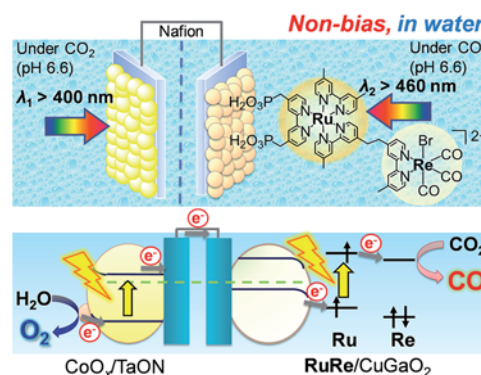


Fig. 8 Schematic image of the hybrid photoelectrochemical cell in a Z-scheme configuration.



light irradiation for a total of 2 h. Fig. 9 shows the time courses of the photocurrent and electrode potentials (a) and the chemical products (b). The generation of a photocurrent and a corresponding increase in the products were clearly observed under irradiation, and the working potential of the electrodes was confirmed to be around +0.15 V vs. Ag/AgCl, at which point both of the photoelectrodes could generate a photocurrent under irradiation *via* the respective half reactions. The products of the reduction (CO and H₂) and oxidation (O₂) were detected in the cathode and anode chambers, respectively (Fig. S10†). A total of 232 nmol of CO was produced, and the TON_{CO} reached 22 based on the amount of immobilized RuRe before the irradiation. The total faradaic efficiency of the cathodic reaction, including the evolution of H₂ (311 nmol), was 72%, whereas that of the anodic reaction was 70% (266 nmol O₂). Notably, an electron balance between the reduction products (CO and H₂) and the oxidation product (O₂) was almost acquired in this photoelectrochemical reaction, while in the case of the corresponding system using the NiO electrode instead of CuGaO₂, there were much less reduction products than the produced O₂.³² The slight decrease in the half amount of electrons when the light was cut in Fig. 9(b) means that a reverse current flowed, which was possibly derived from the discharge of the electrical double layers of the electrodes. When only the cathode or the anode was irradiated, the photocurrent was relatively small in comparison to that when both of the electrodes were under irradiation (Fig. S11†), which suggests that photoexcitation of both of the electrodes is required for the subsequent progress of the photochemical reduction of CO₂ with water as the reductant. On the basis of these data, we conclude that this hybrid photoelectrochemical cell can drive both the reduction of CO₂ and the oxidation of water by the stepwise photoexcitation of RuRe and TaON, *i.e.*, *via* Z-scheme-type electron transfer, which gives CO and O₂ under visible-light irradiation. This is the first successful instance of the reduction of CO₂ in the absence of electrical or chemical bias using visible light and water alone by a hybrid photocatalytic system consisting of a molecular photocatalyst and a semiconductor photocatalyst. Further investigations for the improvement of the efficiency and durability of the photoelectrochemical cell are currently under way in our laboratory.

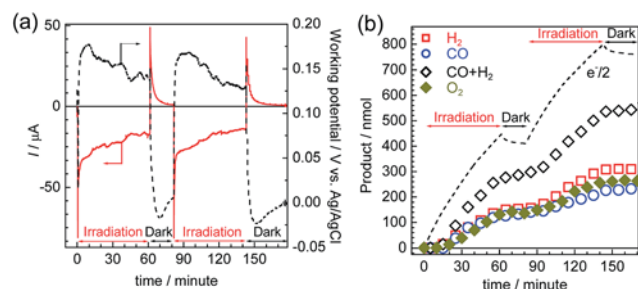


Fig. 9 Time courses of the photocurrent and working potential of the electrodes (a) and the chemical products (b) during the visible-light irradiation of the photoelectrochemical cell consisting of the RuRe/CuGaO₂ photocathode and the CoO_x/TaON photoanode under short-circuit conditions.

Experimental

Synthesis of CuGaO₂ particles

Particles of CuGaO₂ powder were prepared using a solid-state reaction method. The precursor materials, *i.e.*, Cu₂O (Kanto Chemicals, >92%) and Ga₂O₃ (Wako Chemicals, 99.99%), were mixed using an agate mortar. The molar ratio of the precursors was set at Cu : Ga = 1 : 1. The obtained mixture was calcined with a N₂ flow of 100 mL min⁻¹ at 1373 K for 5 h to give a polycrystalline powder of CuGaO₂.

Fabrication of CuGaO₂ electrodes

Fluorine-doped tin oxide (FTO) glass (AGC Fabritech, 15 × 50 mm, 12 Ω sq⁻¹) was sonicated in acetone for 10 min and in methanol for 10 min before use. A suspension of 30 mg of CuGaO₂ powder in 300 μL of isopropanol was prepared with sonication for 10 min. Then, 100 μL of the suspension was dropped onto an exposed area of the FTO glass (*ca.* 5 cm²) and dried in air at room temperature using a drop-casting method and Scotch mending tape as a masking material. The obtained sample was calcined at 773 K for 3 h with a N₂ flow of 100 mL min⁻¹. The electrode was cut in half before use. The amount of powder that was deposited was estimated to be approx. 5 mg for each electrode (*ca.* 2.5 cm²).

Preparation of the hybrid photocathode by the adsorption of the metal complex on the CuGaO₂ electrode

RuRe and its model complexes (Ru and Re) (Chart 1) were synthesized in accordance with reported procedures.⁴³ A CuGaO₂ electrode was immersed in an acetonitrile solution containing the metal complex (4 mL, 5 μM) overnight. The electrode was washed with acetonitrile after the adsorption procedure. The amount of the metal complex that was adsorbed was estimated from the difference in the absorbance between the solutions at 461 nm before and after the hybridization procedures.

Preparation of the CoO_x/TaON photoanode

The CoO_x/TaON electrode was prepared in accordance with a reported procedure.⁴⁶ The outline of the procedure is as follows. TaON powder was prepared by heating Ta₂O₅ powder with an NH₃ flow (20 mL min⁻¹) at 1123 K for 15 h. CoO_x nanoparticles (5 wt% as the metal) were loaded onto the TaON particles *via* impregnation from an aqueous Co(NO₃)₂ solution, followed by heating at 673 K for 30 min in air. The as-prepared CoO_x-loaded TaON particles were deposited on a Ti substrate using electrophoretic deposition. The electrodes were treated with 50 μL of a solution of TaCl₅ in methanol (10 mM) and then dried in air at room temperature. After this process had been performed five times, the electrode was heated in an NH₃ flow (10 mL min⁻¹) at 723 K for 30 min. The details of the structural characterization of the electrode are shown in our previous paper.



Photoelectrochemical measurements and reduction of CO₂ using the RuRe/CuGaO₂ photocathode

A three-electrode setup with an HZ-7000 potentiostat (Hokuto Denko) was used throughout the photoelectrochemical measurements and half reactions. A 50 mM aqueous solution of NaHCO₃ saturated with CO₂ (pH 6.6) was used as an electrolyte. A Pt wire and Ag/AgCl in a saturated aqueous solution of KCl were employed as the counter and reference electrodes, respectively. The counter electrode was separated from the reaction solution using Vycor glass to avoid the influence of the oxidation reaction taking place on the counter electrode. The working electrode (*ca.* 2.5 cm²) was irradiated using a 300 W Xe lamp (Asahi Spectra MAX-302) with an IR-blocking mirror module. A cutoff filter (HOYA Y48 for irradiation at $\lambda_{\text{ex}} > 460$ nm) or a band-pass filter (Asahi Spectra, for the IPCE measurements) was employed to control the irradiation wavelength. The potential against a reversible hydrogen electrode (RHE) (see Fig. 1) was calculated using the Nernst equation (eqn (1)):

$$E \text{ (V vs. RHE)} = E \text{ (V vs. Ag/AgCl)} + 0.199 + 0.059 \text{ pH.} \quad (1)$$

The dependence on the wavelength of the IPCE at a given wavelength was calculated using eqn (2):

$$\text{IPCE (\%)} = [(1240/\lambda_{\text{ex}})(I_{\text{light}} - I_{\text{dark}})/P_{\text{light}}] \times 100, \quad (2)$$

where λ_{ex} and P_{light} are the wavelength and power density of the incident light (nm and $\mu\text{W cm}^{-2}$), respectively, I_{light} is the current density under irradiation ($\mu\text{A cm}^{-2}$), and I_{dark} is the current density in the dark ($\mu\text{A cm}^{-2}$).

The photoelectrochemical reduction of CO₂ was conducted using a Pyrex cell sealed with an O-ring and a stirring tip. The total volume of the cell without the stirring tip and electrodes was *ca.* 130 mL, and 84 mL of the electrolyte solution was utilized; therefore, the estimated volume of the gas phase was *ca.* 46 mL. The reaction was conducted after purging the system with CO₂ for more than 40 min. A cutoff filter (HOYA Y48) was employed for irradiation at $\lambda_{\text{ex}} > 460$ nm. Product analyses of CO and H₂ in the gas phase and HCOOH in the liquid phase were performed using a gas chromatograph (Inficon MGC3000A) and a Capi-3300I capillary electrophoresis system (Otsuka Electronics), respectively. ¹³CO₂ (CIL, ¹³C = 99%) and NaH¹³CO₃ (Aldrich, ¹³C = 99%) were utilized for the labeling experiments. Gas chromatography-mass spectrometry (GC-MS) analysis of the gas phase was conducted using a gas chromatograph equipped with a mass spectrometer (Shimadzu GCMS-QP2010 Ultra).

Photoelectrochemical reduction of CO₂ using the hybrid electrochemical cell in the Z-scheme configuration

The reaction was conducted using a Pyrex cell with two chambers (*ca.* 27 mL for each chamber) that were divided by a Nafion 117 membrane (Aldrich), and the photoelectrodes were installed into each chamber and the cell was sealed with an O-ring. Ag/AgCl in a saturated aqueous solution of KCl was

employed as the reference electrode and was placed into the cathode chamber. A 14.5 mL portion of a 50 mM aqueous solution of NaHCO₃ was added as an electrolyte to each chamber, which was purged with CO₂. A three-electrode setup with an HZ-7000 potentiostat (Hokuto Denko) was used in non-resistance ammeter mode. The RuRe/CuGaO₂ photocathode (*ca.* 3.2 cm², RuRe 10.5 nmol) was irradiated at $\lambda_{\text{ex}} > 460$ nm using a 300 W Xe lamp (Eagle Engineering) with a cutoff filter (HOYA Y48) and a cold mirror (CM-1). The CoO_x/TaON photoanode (*ca.* 3.3 cm²) was irradiated at $\lambda_{\text{ex}} > 400$ nm using a 300 W Xe lamp (Asahi Spectra MAX-302) with a cutoff filter (HOYA L42) and an IR-blocking mirror module. The analysis of gas products was performed using gas chromatography (Inficon MGC3000A).

Characterizations

UV-vis diffuse reflectance spectra were recorded using a V-565 spectrophotometer (JASCO) that was equipped with an integral sphere unit. X-ray diffraction (XRD) patterns were recorded using a MiniFlex600 X-ray diffractometer (Rigaku) that was equipped with monochromatic Cu K α radiation and operated at 15 mA and 40 kV. The scanning electron microscopy (SEM) observations were conducted using an S-4700 microscope (Hitachi High-Tech). An ECSA-3400 X-ray photoelectron spectrometer (Shimadzu) was utilized for the X-ray photoelectron spectroscopy (XPS) measurements. The binding energies were corrected using the C 1s peak (284.6 eV) for each sample.

Conclusions

A novel hybrid photocathode consisting of a CuGaO₂ p-type semiconductor and a RuRe supramolecular complex has been developed for the photoelectrochemical reduction of CO₂ in aqueous solution. The RuRe/CuGaO₂ photocathode displayed photoelectrochemical activity for the conversion of CO₂ to CO in an aqueous electrolyte solution with an onset potential of +0.3 V vs. Ag/AgCl. A photoelectrochemical cell comprising the RuRe/CuGaO₂ photocathode and a CoO_x/TaON photoanode exhibited activity for the visible-light-driven reduction of CO₂ using water as a reductant to generate CO, H₂, and O₂ with no external bias.

Acknowledgements

This work was supported by JSPS KAKENHI Grant Number JP24107005 in Scientific Research on Innovative Areas "Artificial Photosynthesis (AnApple)", the Strategic International Collaborative Research Program (SICORP) from JST, and JST CREST Grant Number JPMJCR13L1 in "Molecular Technology". H. K. thanks JSPS KAKENHI Grant Number JP16K21031 for Young Scientists (B) and K. M. thanks JSPS KAKENHI Grant Number JP16H06441 in Scientific Research on Innovative Areas "Mixed Anion" for their financial support. We thank Prof. Kazunari Domen from the University of Tokyo for the SEM measurements.



Notes and references

- 1 A. J. Morris, G. J. Meyer and E. Fujita, *Acc. Chem. Res.*, 2009, **42**, 1983–1994.
- 2 G. Sahara and O. Ishitani, *Inorg. Chem.*, 2015, **54**, 5096–5104.
- 3 Y. Yamazaki, H. Takeda and O. Ishitani, *J. Photochem. Photobiol., C*, 2015, **25**, 106–137.
- 4 A. Nakada, K. Koike, T. Nakashima, T. Morimoto and O. Ishitani, *Inorg. Chem.*, 2015, **54**, 1800–1807.
- 5 A. Nakada, K. Koike, K. Maeda and O. Ishitani, *Green Chem.*, 2016, **18**, 139–143.
- 6 B. Gholamkhash, H. Mametsuka, K. Koike, T. Tanabe, M. Furue and O. Ishitani, *Inorg. Chem.*, 2005, **44**, 2326–2336.
- 7 S. Sato, K. Koike, H. Inoue and O. Ishitani, *Photochem. Photobiol. Sci.*, 2007, **6**, 454–461.
- 8 K. Koike, S. Naito, S. Sato, Y. Tamaki and O. Ishitani, *J. Photochem. Photobiol., A*, 2009, **207**, 109–114.
- 9 Y. Tamaki, T. Morimoto, K. Koike and O. Ishitani, *Proc. Natl. Acad. Sci. U. S. A.*, 2012, **109**, 15673–15678.
- 10 Y. Tamaki, K. Watanabe, K. Koike, H. Inoue, T. Morimoto and O. Ishitani, *Faraday Discuss.*, 2012, **155**, 115–127.
- 11 Y. Tamaki, K. Koike, T. Morimoto and O. Ishitani, *J. Catal.*, 2013, **304**, 22–28.
- 12 Y. Tamaki, K. Koike, T. Morimoto, Y. Yamazaki and O. Ishitani, *Inorg. Chem.*, 2013, **52**, 11902–11909.
- 13 E. Kato, H. Takeda, K. Koike, K. Ohkubo and O. Ishitani, *Chem. Sci.*, 2015, **6**, 3003–3012.
- 14 Y. Tamaki, K. Koike and O. Ishitani, *Chem. Sci.*, 2015, **6**, 7213–7221.
- 15 T. Arai, S. Sato, K. Uemura, T. Morikawa, T. Kajino and T. Motohiro, *Chem. Commun.*, 2010, **46**, 6944.
- 16 S. Sato, T. Arai, T. Morikawa, K. Uemura, T. M. Suzuki, H. Tanaka and T. Kajino, *J. Am. Chem. Soc.*, 2011, **133**, 15240–15243.
- 17 T. Arai, S. Tajima, S. Sato, K. Uemura, T. Morikawa and T. Kajino, *Chem. Commun.*, 2011, **47**, 12664–12666.
- 18 T. Arai, S. Sato, T. Kajino and T. Morikawa, *Energy Environ. Sci.*, 2013, **6**, 1274–1282.
- 19 K. Maeda, K. Sekizawa and O. Ishitani, *Chem. Commun.*, 2013, **49**, 10127–10129.
- 20 K. Maeda, R. Kuriki, M. Zhang, X. Wang and O. Ishitani, *J. Mater. Chem. A*, 2014, **2**, 15146–15151.
- 21 T. Arai, S. Sato and T. Morikawa, *Energy Environ. Sci.*, 2015, **8**, 1998–2002.
- 22 R. Kuriki, K. Sekizawa, O. Ishitani and K. Maeda, *Angew. Chem., Int. Ed.*, 2015, **54**, 2406–2409.
- 23 K. Maeda, R. Kuriki and O. Ishitani, *Chem. Lett.*, 2016, **45**, 182–184.
- 24 R. Kuriki, O. Ishitani and K. Maeda, *ACS Appl. Mater. Interfaces*, 2016, **8**, 6011–6018.
- 25 K. Sekizawa, K. Maeda, K. Domen, K. Koike and O. Ishitani, *J. Am. Chem. Soc.*, 2013, **135**, 4596–4599.
- 26 F. Yoshitomi, K. Sekizawa, K. Maeda and O. Ishitani, *ACS Appl. Mater. Interfaces*, 2015, **7**, 13092–13097.
- 27 A. Nakada, T. Nakashima, K. Sekizawa, K. Maeda and O. Ishitani, *Chem. Sci.*, 2016, **7**, 4364–4371.
- 28 R. Kuriki, H. Matsunaga, T. Nakashima, K. Wada, A. Yamakata, O. Ishitani and K. Maeda, *J. Am. Chem. Soc.*, 2016, **138**, 5159–5170.
- 29 K. Muraoka, H. Kumagai, M. Eguchi, O. Ishitani and K. Maeda, *Chem. Commun.*, 2016, **52**, 7886–7889.
- 30 K. Wada, M. Eguchi, O. Ishitani and K. Maeda, *ChemSusChem*, 2017, **10**, 287–295.
- 31 G. Sahara, R. Abe, M. Higashi, T. Morikawa, K. Maeda, Y. Ueda and O. Ishitani, *Chem. Commun.*, 2015, **51**, 10722–10725.
- 32 G. Sahara, H. Kumagai, K. Maeda, N. Kaeffer, V. Artero, M. Higashi, R. Abe and O. Ishitani, *J. Am. Chem. Soc.*, 2016, **138**, 14152–14158.
- 33 J. He, H. Lindström, A. Hagfeldt and S.-E. Lindquist, *J. Phys. Chem. B*, 1999, **103**, 8940–8943.
- 34 N. Kaeffer, J. Massin, C. Lebrun, O. Renault, M. Chavarot-Kerlidou and V. Artero, *J. Am. Chem. Soc.*, 2016, **138**, 12308–12311.
- 35 S. Nandy, A. Banerjee, E. Fortunato and R. Martins, *Rev. Adv. Sci. Eng.*, 2013, **2**, 273–304.
- 36 H. Kawazoe, M. Yasukawa, H. Hyodo, M. Kurita, H. Yanagi and H. Hosono, *Nature*, 1997, **389**, 939–942.
- 37 H. Yanagi, H. Kawazoe, A. Kudo, M. Yasukawa and H. Hosono, *J. Electroceram.*, 2000, **4**, 407–414.
- 38 K. Ueda, T. Hase, H. Yanagi, H. Kawazoe, H. Hosono, H. Ohta, M. Orita and M. Hirano, *J. Appl. Phys.*, 2001, **89**, 1790–1793.
- 39 A. Renaud, B. Chavillon, L. Le Pleux, Y. Pellegrin, E. Blart, M. Boujtita, T. Pauporté, L. Cario, S. Jobic and F. Odobel, *J. Mater. Chem.*, 2012, **22**, 14353–14356.
- 40 M. Yu, G. Natu, Z. Ji and Y. Wu, *J. Phys. Chem. Lett.*, 2012, **3**, 1074–1078.
- 41 J. W. Lekse, M. K. Underwood, J. P. Lewis and C. Matranga, *J. Phys. Chem. C*, 2012, **116**, 1865–1872.
- 42 M. Lee, D. Kim, Y. T. Yoon and Y. Il Kim, *Bull. Korean Chem. Soc.*, 2014, **35**, 3261–3266.
- 43 Y. Ueda, H. Takeda, T. Yui, K. Koike, Y. Goto, S. Inagaki and O. Ishitani, *ChemSusChem*, 2015, **8**, 439–442.
- 44 The value of $E_{1/2}^{*red}$ of **RuRe** was calculated using the reported values of $E_{1/2}^{red}$ and E_{00} from ref. 31 and was converted to potential vs. Ag/AgCl.
- 45 Y. Kuramochi and O. Ishitani, *Inorg. Chem.*, 2016, **55**, 5702–5709.
- 46 M. Higashi, K. Domen and R. Abe, *J. Am. Chem. Soc.*, 2012, **134**, 6968–6971.

